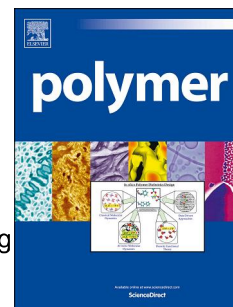# Accepted Manuscript

Design of low temperature-responsive hydrogels used as a temperature indicator

Li Tang, Liang Gong, Guiyin Zhou, Lingyun Liu, Dong Zhang, Jianxin Tang, Jie Zheng

Design of Low Temperature-Responsive Hydrogels Used as a Temperature Indicator

Li Tang[1,2,3], Liang Gong[1], Guiyin Zhou[1], Lingyun Liu[3], Dong Zhang[3], Jianxin Tang[1*], and Jie Zheng[3*]

[1] Hunan Key Laboratory of Biomedical Nanomaterials and Devices
College of Life Sciences and Chemistry
Hunan University of Technology, Zhuzhou 412007, China

[2] College of Packaging and Material Engineering
Hunan University of Technology, Zhuzhou 412007, China

[3] Department of Chemical & Biomolecular Engineering
The University of Akron, Akron, Ohio 44325, USA

Corresponding Authors: (J.T.) jxtang0733@163.com; (J. Z.)zhengj@uakron.edu;

Abstract

Development of highly thermo-sensitive hydrogels, particularly at a low-temperature range, has promising applications in diverse fields. Herein we designed, synthesized, and characterized tri-copolymer poly(N-tert-butyl acrylamide-*co*-N-isopropyl acrylamide-*co*-acrylamide) p(NTBAM-co-NIPAM-co-AM) hydrogels using a facile one-pot method. The copolymerization of two thermo-responsive monomers of NTBAM and NIPAM with hydrophilic AM monomers aimed to tune the temperature range of lower critical solution temperature (LCST) between 8□-10 □ by varying the concentrations and molar ratios of NTBAM, NIPAM, and AM. At optimal conditions, p(NTBAM-co-NIPAM-co-AM) hydrogels showed a rapid and large deswelling by reducing their original sizes by 21 % in 2 min as temperature was slightly changed from 8 □ to 10 □. Such low-temperature-triggered de-swelling behavior and tunable LCST property are likely attributed to delicate interplay between different network components and their interactions with water. Due to high temperature sensitivity (~2 □), large volume deswelling ratio (90%), and low temperature-responsive range (8-10 □), we further demonstrated a prototype hydrogel ball actuator as temperature indicator to monitor minor temperature-induced size changes. The design strategy for this p(NTBAM-co-NIPAM-co-AM) hydrogel could be generally applicable to other thermo-responsive hydrogels with different shapes and temperature-responsive ranges, which could be used as low-temperature indicator for many applications including vaccine storage and transportation.

Keywords: Hydrogel; Vaccine; Polyacrylamide; Stimuli-Response;

Introduction

Since the first smallpox vaccine was discovered in 18th century,[1, 2] developing vaccines for immune therapy has been considered as the most promising therapeutics strategy against many human diseases. Global Alliance for Vaccines and Immunizations (GAVI) estimates that approximately three million people are saved by vaccines every year.[3] On the other hand, considering that vaccines are extremely sensitive to the storage and transportation environment (particularly temperature), high temperatures often cause rapid denaturation and degradation of proteins or carbohydrate-based antigens in vaccines,[4] while low temperatures may also produce the formation of ice crystals that will in turn alter the conformation of antigens and the binding of vaccine–adjuvant complexes.[5] Thus, vaccines need to be stored, transported, and used at proper conditions to maintain their activities, particularly a very narrow temperature range of 2–8 □ (namely cold chain refrigeration) is necessary to preserve the immunogenicity of most vaccines (e.g. tetanus toxoid, anthrax, diphtheria, acellular pertussis, and hepatitis B[6, 7]). It was reported that ~50% of vaccines were finally discarded due to their poor thermal stability.[8] Such temperature-sensitivity of vaccines greatly limits their widespread applications. Therefore, it is equally important but has proved to be challenging to develop both novel vaccines and new technologies/materials for safely deliver, store, and real-time monitor vaccines at proper conditions.

Various approaches have been developed to realize the real-time monitoring of vaccine temperature, including vaccine vial monitor (VVM) sticker, electronic temperature recorder (ETR), cold chain monitor, and electronic freeze indicators.[9-11] Among them, developing thermo-responsive materials has great advantages for real-time monitoring vaccine temperature in any stage involving production, transportation, and storage. Temperature-responsive hydrogels have been widely used as smart materials [12-19]. Most of temperature-responsive hydrogels, such as poly(N-isopropylacrylamide) (pNIPAM) hydrogels, undergo volume changes due to the lower critical solution temperature (LCST),[20-22] i.e. temperature-responsive hydrogels swell at temperatures of <LCST, but shrink at temperatures of >LCST. The sol-gel LCST temperatures can be tuned by altering the degree of polymerization,[23] incorporating other composites,[24] or co-polymerizing with other polymers,[25] all of which can change the LCST–UCST properties. For instance, the copolymerization of hydrophilic N,N-dimethylaminopropylacrylamide (DMAPAAm) with NIPAM enhance hydrogen bonds between polymer chains and water molecules, leading to the increase of LCST for p(NIPAM-co-DMAPAAM) copolymers.[26-28] Differently, when copolymerizing hydrophobic butyl methacrylate(BMA) with NIPAM, p(NIPAM-co-BMA) copolymer reduced its LCST as compared to pure NIPAM.[29-31]

However, most of existing temperature-responsive hydrogels, including polysaccharides,[32, 33] N-isopropylacrylamide copolymer,[34-36] PEG/PPO block

copolymers and their derivatives,[37, 38] PEG/PLGA block copolymers[39, 40], and thermosensitive liposomes[41, 42] still require high temperatures (above vaccine storage temperature of 2-8 ℃) to trigger responses. To overcome this limit, herein we reported a simply one-pot thermal initiated free radical polymerization method to design and synthesis of temperature-responsive poly(N-tert-butyl acrylamide-co-N-isopropyl acrylamide-co-acrylamide) p(NTBAM-co-NIPAM-co-AM) hydrogels for real-time monitoring vaccine temperatures around 2-8□. Since both NTBAM and NIPAM are temperature-sensitive monomers with respective LCST of -5 °C and 32 °C, the copolymerization of NTBAM and NIPAM enabled to create a relatively wide range of temperatures (-5 °C-32 °C) for p(NTBAM-co-NIPAM-co-AM) hydrogels to change their volume via swelling or shrining. Moreover, while hydrophilic AM as the third component does not possess any temperature-induced property (e.g. phase transition and volume change), the introduction of AM into p(NTBAM-co-NIPAM) network can help to tune the LCST towards the even lower range of 6 °C-18 °C, covering a safe temperature range of vaccines. As a conceptual example, an as-prepared hydrogel was fabricated into a soft sphere with a diameter of 2.1 cm (larger than a typical size of bottleneck (1.7 cm in diameter) of vaccine containers) at temperature of <8 ℃. As temperature increased above 8 □, the hydrogel ball shrank to a smaller diameter of 1.5 cm so as to pass through the bottleneck and drop into the bottle. The design strategy could be generally applicable to other thermo-responsive hydrogels with different shapes and temperature-responsive ranges, which could be used as temperature indicators for different applications in food processing and production, biotechnology storage, and cold chain warehouse.

Materials and Methods

Reagents. N-tert-butyl acrylamide (NTBAM, 97%), N-isopropyl acrylamide (NIPAM, 98%), acrylamide (AM, 99%), N, N'-methylenebisacrylamide (MBA, 99%) and potassium persulfate (KPS, 98%) all were purchased from J&K chemical, and without further purification. Tert-Butanol was obtained from Sinoreagent. Deionized water (18.2MΩ) used in this study was generated by Milli-Q system.

Hydrogel synthesis. The low temperature-responsive hydrogel was synthesized by a traditional free-radical crosslinking copolymerization following this protocol: monomers including N-tert-butyl acrylamide (5.25 mmol, 0.667 g), N-isopropyl acrylamide (1.50 mmol, 0.17 g), acrylamide (2.5 mmol, 0.178 g) and cross-linker N, N'-methylenebisacrylamide (MBA, 18 mg) joined into 10 ml mixture solution contains tert-butanol (5 ml) and deionized water (5 ml), then stirred to dissolve all the reactant and produced a transparent solution. After that, initiator (KPS) was added to this transparent solution for polymerization at 60 °C for 12 h in a tube whose diameter is 1.2 cm. After the copolymerization, the as-prepared hydrogel was cut into disc (1.2 cm in diameter and about 2 mm in thickness) and immersed in deionized water in refrigerator to get equilibrium swelling. The soak solution was refreshed three times to remove non-reacted reactants.

4

Scanning Electron Microscopy (SEM). The morphology and microscopy of dry hydrogels were checked by scanning electron microscopy (TESCAN MIRA3 LMU). Hydrogel discs were first immersed in deionized water at 4 ℃ in the refrigerator for swelling to reach equilibrium. Then put the swelling disc hydrogel into 10 ℃ water bath to de-swelling at equilibrium. The same method treated another hydrogel at 26 ℃. Subsequently frozen these hydrogels by liquid nitrogen at -196 ℃. The frozen samples were dried in a freeze drier for 36 h at -50 ℃.

Fourier-Transform Infrared Spectroscopy (FTIR). FT-IR spectra were record on Thermo Fisher Nicolet 380 in the range 400-4000 cm^{-1} with a resolution at 4 cm^{-1}. The dried hydrogel or monomer was ground to powder and then mixed with KBr to press into a tablet.

Differential Scanning Calorimeter (DSC). DSC of dry p(NTBAM-co-NIPAM-co-AM) hydrogels (8 mg) was performed in nitrogen-protected environment using a Q-20 apparatus from -50 to 300 ℃. The dry hydrogel samples were first heated up to 300 ℃ at rate of 20 ℃/min to remove the thermal history and then cooled down to -50 ℃. Then, the second heating run was performed at 10 ℃/min from -50 to 300 ℃ to determine glass transition temperature (T_g).

Swelling behavior. Swelling ratio of hydrogels was measured by the volume change between as-prepared gel and a swelling gel in DI water at 10 ℃ and different immerse times, as shown in Equation 1.

$$SR = \frac{D_t}{D_0} \quad (1)$$

where D_0 is an initial diameter of as-prepared hydrogel and D_t is an equilibrium diameter of swollen hydrogel at different immerse times.

Deswelling test. Volume shrank can be represented by changes in diameter. The deswelling behaviors of hydrogel sample was measured at temperature range from 2 ℃ to 26 ℃ in the temperature-controlled biochemical incubator. In order to reach equilibrium swelling, hydrogel discs were immersed in water at refrigerator for 24 h. During the test, incubator temperature was increased 2 ℃ each time, and keep temperature for 2 h at different temperature. The volume deswelling ratio of the hydrogel q can be calculated by

$$q = 1 - \left(\frac{D}{D_0}\right)^3 \quad (2)$$

where D_0 is the diameter of equilibrium swelling hydrogel, D is the hydrogel diameter deswelling at different temperature.

Compression testing. Uniaxial compression tests were performed on a universal

5

tensile tester (Instron 3345, MA). Cylindrical as-prepared hydrogel samples were cut into 10-15 mm thick with a diameter of 10 mm. The compressive stress (σ) was calculated by

$$\sigma = \frac{F}{\pi r^2} \quad (3)$$

where r is the initial unloaded radius and F is the loading force.

Crosslink density. The compression modulus (G) was obtained by linear dependence from the slope of τ versus (λ-λ^{-2}) according the Eq. (4).[43]

$$\tau = G(\lambda - \lambda^{-2}) \quad (4)$$

The volume fraction of the copolymer in the hydrogel was calculated from Eq. (5):

$$\varphi = \frac{V_d}{V} \quad (5)$$

V_d is volume of dry hydrogel, V is volume of hydrogel swelling to equilibrium at 4 □, and according Huglin theory, compression modulus(G) can be evaluated from the effective crosslink density(v_e) and the molar mass between crosslinks(M_c) via Eq. (6) and Eq. (7), respectively:

$$M_c = \rho/v_e \quad (6)$$
$$v_e = G\varphi^{1/3}/RT \quad (7)$$

Substituting Eq. (7) into Eq. (6), then obtains the following equation.

$$M_c = \rho RT/G\varphi^{1/3} \quad (8)$$

The theoretical crosslink density (v_t) was given by Eq. (9):

$$v_t = Cf/2 \quad (9)$$

In which C is the concentration of cross-linker MBA concentration and f is the crosslinker functionality. In this case, MBA with a functionality of 4 was selected as crosslinker.

Results and Discussion

Figure 1 shows a synthesis process of p(NTBAM-co-NIPAM-co-AM) hydrogel. Briefly, all reactants of NTBAM, NIPAM, AM monomers and MBA crosslinker (except for KPS) were well mixed in water, then the mixture solution was heated up to 60 °C for dissolving all reactants, producing a transparent solution. After that, initiator (KPS) was added to this transparent solution for polymerization at 60 °C for 12 h in a spherical mold. During this gelation process, the p(NTBAM-co-NIPAM1-co-AM) network was formed and crosslinked by MBA, and the transparent solution gradually became a milky, spherical gel with an initial diameter of 1.2 cm. Upon immersing the as-prepared p(NTBAM-co-NIPAM1-co-AM) gel in water, the diameter of the swollen hydrogel increased from 1.2 cm to 2.1 cm at 4□. At temperatures of <8 □, the swollen hydrogel ball retained its diameter of 2.1 cm, which was larger than a bottleneck diameter of 1.7 cm. But, as temperature increased above 8 □, the hydrogel ball shrank to a smaller diameter of <1.7 cm so as to pass through the bottleneck and drop into the bottle.

Taking advantage of this unique LCST-induced sol-gel transition feature of p(NTBAM-co-NIPAM-co-AM) hydrogel, the hydrogels were designed and prepared at 0.525 mmol/ml of NTBAM, 0.15 mmol/ml of NIPAM, 0.25 mmol/ml of AM to realize temperature-stimuli, controllable swelling actuation. **Fig. 2a** shows the deswelling behaviors of p(NTBAM-co-NIPAM-co-AM) hydrogel as temperature, showing a three-stage time-dependent shrinking behavior. At the initial stage of temperature change from 2-6 ⌐, the hydrogel remained its initial size almost unchanged at a diameter of 2.1 cm. Then, the hydrogel underwent a rapid size decrease from 2.1 to 1.2 cm as temperature was increased from 6 to 12 ⌐. Finally, the continuous increase of temperature from 12 to 26 ⌐ led the hydrogel to slowly reduce its size from 1.2 to 1.0 cm. So, p(NTBAM-co-NIPAM-co-AM) hydrogel exhibited a cold-chain temperature-responsive range of 6-12 ▢. Such temperature-induced shrinking behavior is caused by the LCST transition from hydrophilicity (swollen state) to hydrophobicity (collapsed state) in thermo-responsive p(NTBAM-co-NIPAM-co-AM) hydrogel, resulting in the loss of water. **Fig. 2b** showed that only at an optimal temperature range of 8-10 ⌐, the hydrogel displayed the largest volume changes up to 0.4 cm, while too high (>10 ⌐) or too low (<8 ⌐) temperatures only led to very slight or negligible size changes (<0.3 cm).

We also studied the swelling kinetics of pNTBAM, pNIPAM, and p(NTBAM-co-NIPAM-co-AM) hydrogels in DI water at 10 ⌐ (**Figure 2c**). It can be seen that as immersion time increased from 0 to 100 min, pNTBAM hydrogel is almost non-swellable and did not show obvious volume change, and this could be attributed to the strong hydrophobic capacity of t-butyl groups for preventing water transportation from outside to the interior of the hydrogel. In sharp contrast, both pNIPAM and p(NTBAM-co-NIPAM-co-AM) hydrogels exhibited obvious swelling behaviors as immersion time, but pNIPAM hydrogel showed the higher swelling ratios than p(NTBAM-co-NIPAM-co-AM) hydrogel across an entire range of immerse time. This is not surprising that the enhanced the cross-link density of p(NTBAM-co-NIPAM-co-AM) gel by cross-linking of multiple polymeric chains constraint the expansion of polymer network, consistent with the SEM results shown in **Figure 3**.

Since both pNTBAM and pNIPAM have a thermo-sensitivity, with different LCST of -5 ∟ and 32 ⊔, respectively, we further compared the component effect on the LCST changes between both p(NTBAM-co-NIPAM-co-AM) and p(NTBAM-co-AM) hydrogels. For comparison, a series of p(NTBAM-co-AM) hydrogels were fabricated with different C_{NTBAM}/C_{AM} molar concentration ratios (**Table S1**) and all of them showed a three-stage deswelling behaviors (**Figure S1**) similar to p(NTBAM-co-NIPAM-co-AM) hydrogels. P(NTBAM-co-AM) hydrogels prepared at C_{NTBAM}/C_{AM} of 1.5 showed a slow deswelling behaviors, as evidenced by smaller changes from 2.1 cm to 1.2 cm at 6-18 ⊔ and from 1.2 cm to 0.9 cm at 18-26 ⊔, respectively. Similar deswelling behaviors was also observed at different molar ratios from 1.27 to 1.63. In parallel, the effect of monomer concentrations on

7

hydrogel deswelling behaviors was also examined by varying total monomer mass percentage of 8-14 wt% while keeping constant concentrations of NTBAM at 0.6 mmol/ml and AM at 0.4 mmol/ml (**Figure S2**). The results indicate that the deswelling behaviors appear not to strongly depend on their concentrations. Comparing the deswelling behaviors of p(NTBAM-co-NIPAM-co-AM) and p(NTBAM-co-AM) hydrogels, the results indicate that the incorporation of hydrophilic NIPAM into p(NTBAM-co-AM) network increases hydrophilic content, making p(NTBAM-co-NIPAM-co-AM) hydrogel a faster deswelling behaviors and more adjustable LCST than p(NTBAM-co-AM) hydrogel.

SEM images were further used to characterize the interior network morphologies of freeze-dried p(NTBAM-co-NIPAM-co-AM) hydrogels, which were obtained by swelling at 4 ⊔ and then deswelling at different temperatures of 4 ⌐, 10 ⌐ and 26 ☐. In general, as shown in **Figure 3**, while all p(NTBAM-co-NIPAM-co-AM) hydrogels presented uniform sponge-like structures, they still showed large differences in network porosity and morphology. Specifically, the hydrogels exhibited a much larger and loose cross-sectional structure with ~5.27 μm pore size when deswelling at 4 ⊔ (**Fig. 3a**), but a more compact structure with average pore size of ~2.73 μm at 10 ☐ (**Fig. 3b**). Further increase of deswelling temperature to 26 ☐ led the gel to present a spherical stacking structure, completely different from the former two structures (**Fig. 3c**). This indicate that de-swelling of hydrogels at higher temperatures leads to the smaller and more compact porous structures due to loss of water. Furthermore, **Figure 3d** shows Fourier Transform Infrared (FT-IR) spectrum of AM monomer and p(NTBAM-co-NIPAM-co-AM) polymers. AM monomer showed the two characteristic absorption peaks at 1615 cm^{-1} and 1672 cm^{-1} corresponding to C=C and C=O, respectively. Differently, p(NTBAM-co-NIPAM-co-AM) polymer showed a carbonyl stretching peak at 1636 cm^{-1} at the expense of conversion from olefin double bonds to single bonds.

To better understand the effects of network components on thermal-responsive properties (e.g. LCST and deswelling), we prepared p(NTBAM-co-NIPAM-co-AM) hydrogels under different fabrication conditions of NTBAM from 0.5 mmol/ml to 0.55 mmol/ml, NIPAM from 0.15 mmol/ml to 0.21 mmol/ml, and AM from 0.22 mmol/ml to 0.34 mmol/ml and examined the effect of different monomer ratios on LCST and deswelling properties, and results were summarized in **Figure S4-S5** and **Table S2-S4**. In **Table S2**, as C_{AM}/C_{NIPAM} ratio increased from 1.47 to 1.62, LCST of p(NTBAM-co-NIPAM-co-AM) hydrogel increased from 8 to 18 ⌐, while the size of decreased diameter was reduced from 0.27 to 0.08 cm within a small temperature window of 8-10 °C. As expected, the higher C_{AM}/C_{NIPAM} slowed down the deswelling process (**Figure S4a**). Such slow deswelling behaviors can be attributed to higher conformational freedom of more hydrophilic dangling chains which can bound more free water,[44] resulting in the higher LCST and the stronger hydrogen bonds. Also, a linear relationship between LCST and C_{AM}/C_{NIPAM} was observed (**Fig. S4b**), indicating that polymer chains with the lower LCST are more efficient in accelerating

the deswelling process. Moreover, by varying C_{AM}/C_{NTBAM} ratio, similar temperature-dependent deswelling behaviors of p(NTBAM-co-NIPAM-co-AM) hydrogels was also observed (**Figure S5a**), showing a linear relationship between LCST and C_{AM}/C_{NTBAM} ratio (**Figure S5b**). The increase of C_{AM}/C_{NTBAM} ratio from 0.44 to 0.62 also led to the increase of LCST from 8 to 12 □, and the decrease of hydrogel diameter from 0.27 to 0.1cm when temperature increased from 8 to 10 ⌟, respectively (**Table S3**). Comparison the relationship between LCST and network concentrations (**Figure S4b** and **Figure S5b**) reveals that C_{AM}/C_{NIPAM} appears to have the larger impact on the change of LCST than C_{AM}/C_{NTBAM}, presumably because hydrophilic NIPAM tends to bind to more water molecules tightly than hydrophobic NTBAM. Furthermore, C_{NIPAM}/C_{NTBAM} ratio appeared not to have a major impact on the changes of LCST and hydrogel size in a temperature range of 8-10 □ (**Table S4**), as well as the deswelling curves (**Figure S6a**) and relationship between LCST and C_{NIPAM}/C_{NTBAM} (**Figure S6b**). The combination of hydrophobic NTBAM and hydrophilic NIPAM leads to the increase of hydrophobic interactions between polymer chains, which in turn reduce water binding ability and cause a negligible effect on its LCST change and a faster deswelling. Based on the above-mentioned results, p(NTBAM-co-NIPAM-co-AM) hydrogel, prepared at 0.525 mmol/ml of NTBAM, 0.15 mmol/ml of NIPAM, 0.25 mmol/ml AM, enables to tune LCST to be 8 ⊐ and achieve the largest diameter changes at temperature from 8 □ to 10 □.

We also examined the effect of network components on the glass transition temperature (T_g). Four different hydrogels were prepared at different concentrations of NTBAM, NIPAM, and AM (**Table 1**) to possess different LCST of p(NTBAM-co-NIPAM-co-AM) hydrogels for DSC tests. As shown in **Figure 4a**, DSC curves showed that four p(NTBAM-co-NIPAM-co-AM) hydrogels with different LCST exhibited a similar DSC thermograms curves. As a result, the glass transition temperature of p(NTBAM-co-NIPAM-co-AM) hydrogel increased linearly from 157.7 □ to 161.7 □ as LCST increased from 6 ⊐ to 18 ⊐ (**Figure 4b**). This could be explained that as the AM concentration increased, the interaction of polymer chain was enhanced which resulted a higher T_g.

Figure 5a shows the MBA crosslinker effect on temperature-responsive deswelling behaviors of p(NTBAM-co-NIPAM-co-AM) hydrogels. First, at the four different MBA concentrations of 9-36 mg, all as-synthesized p(NTBAM-co-NIPAM-co-AM) hydrogels shrank as temperatures and displayed similar three-stage deswelling behaviors. Specifically, as temperature increased from 8 to 10 ⊓, p(NTBAM-co-NIPAM-co-AM) hydrogels reduced their sizes by 0.43 cm, 0.42 cm, 0.35 cm, and 0.33 cm at 9, 18, 27, and 36 mg/mL of MBA, respectively (**Figure 5b**). We also performed the compressive tests for p(NTBAM-co-NIPAM-co-AM) hydrogels. **Figure 5c** shows typical compressive stress/strain curves of p(NTBAM-co-NIPAM-co-AM) hydrogels at different MBA crosslinker concentrations (9-36 mg). As crosslinker concentrations increased from 9 mg to 36 mg, compressive stress and strain decreased from 28.89 MPa to 22.82 MPa

and from 0.93 to 0.89, respectively. Increase of crosslinker contents would shorten the effective connections between polymer chains and increase their interactions, thus rendering the hydrogels become more brittle and less swellable. Meanwhile, it can be seen that the larger deformation (strain) of hydrogels, the higher compressive stress and smaller compression modulus (G). Moreover, compression modulus (G) increased as crosslinker contents increased (**Table 1**). Increase of crosslinker contents would shorten the effective connections between polymer chains and increase their interactions, thus rendering the hydrogels become more brittle and less swellable. Comparison of the effective crosslink density(v_e) with the theoretical crosslink density (v_t) in **Table 1** suggests that only ~20~30 % of crosslinkers could form effective chains in the polymer network[45]. Taken together, the as-prepared p(NTBAM-co-NIPAM-co-AM) hydrogels have demonstrated their temperature-responsive properties, with the tunable LCST by changing the concentrations and ratios of network components.

P(NTBAM-co-NIPAM-co-AM) hydrogels demonstrate tunable LCST between 6-18 □ to control their deswelling behaviors. Based on this temperature-responsive deswelling behavior, we further designed a thermo-responsive hydrogel ball, which act as a temperature indicator to monitor temperature changes between 2-8 □ (same as vaccine storage temperature of 2-8 □). As a proof-of-concept example in **Fig. 6**, a hydrogel ball made of p(NTBAM-co-NIPAM-co-AM) with a diameter of 2.1 cm was initially placed in and stuck at a neck of vessel containing water at cold temperatures of <8 □ (**Fig. 6a**). As temperature was slightly increased from 8 □ to 10 □ or above, the hydrogel ball experienced a large and rapid volume shrinkage in 2 min, allowing the ball to fall into the vessel (**Fig. 6b-d**). The volume deswelling ratio was 90%, which outperformed other porous hydrogels (e.g. air-dried polyacrylamide and sodium polyacrylate hydrogels). Such high temperature sensitivity (~2 □), large volume deswelling ratio (90%), and low temperature-responsive range (8-10 □) make p(NTBAM-co-NIPAM-co-AM) hydrogels very promising for real-time monitoring vaccine temperature during the storage and transportation processes.

Conclusions

In this work, we fabricated tri-copolymer p(NTBAM-co-NIPAM-co-AM) hydrogels with tunable, low-temperature-responsive, de-swelling behavior using a facile one-pot free radical copolymerization method. A design strategy for this tri-copolymer system was based on (a) the two thermosensitive monomers of NTBAM and NIPAM to determine the temperature range of the LCST; (b) the hydrophilic monomer of AM to regulate the temperature due to their competitive interactions between p(NTBAM-co-NIPAM) network and water molecules; and (c) the cross-linker of MBA to modulate the swelling degree. By varying the concentrations and ratios of NTBAM, NIPAM, and AM, the optimal p(NTBAM-co-NIPAM-co-AM) hydrogels demonstrated their fast size shrink by 21 % in 2 min as temperature was slightly changed from 8 □ to 10 □ (same as vaccine storage temperature of 2-8 □). Taking advantage such unique de-swelling property, we further designed a

10

temperature-responsive hydrogel actuator, which can be used as low temperature indicator for a variety of applications such as vaccine safety, artificial muscles, and intelligent human-machine interfacial materials.

Table 1. Swelling data and stress-strain measurements data of p(NTBAM-co-NIPAM-co-AM) hydrogel with different MBA concentrations.

Gel*	ρ_d (g/cm^3)	φ	G (KPa)	v_t (mol/cm^3)	v_e (mol/cm^3)	M_c
Gel 9	1.12	1.25×10^{-2}	8.97	1.67×10^{-5}	4.27×10^{-6}	2.62×10^{5}
Gel 18	1.12	1.45×10^{-2}	15.10	3.34×10^{-5}	7.02×10^{-6}	1.59×10^{5}
Gel 27	1.12	1.80×10^{-2}	20.20	5.01×10^{-5}	8.95×10^{-6}	1.25×10^{5}
Gel 36	1.12	2.27×10^{-2}	26.56	6.68×10^{-5}	1.11×10^{-5}	1.01×10^{5}

Gel*: From Gel 9 to Gel 36, Gel 9 means that the MBA usage is 9 mg, and the same as gel 18, gel 27 and gel 36, both gels were prepared under the same monomer concentration of NTBAM = 0.525 mmol/ml, NIPAM = 0.15 mmol/ml, AM = 0.25 mmol/ml and KPS = 5 mg.

Figure 1. Scheme of synthesis low temperature responsive hydrogel ball and temperature monitoring container.
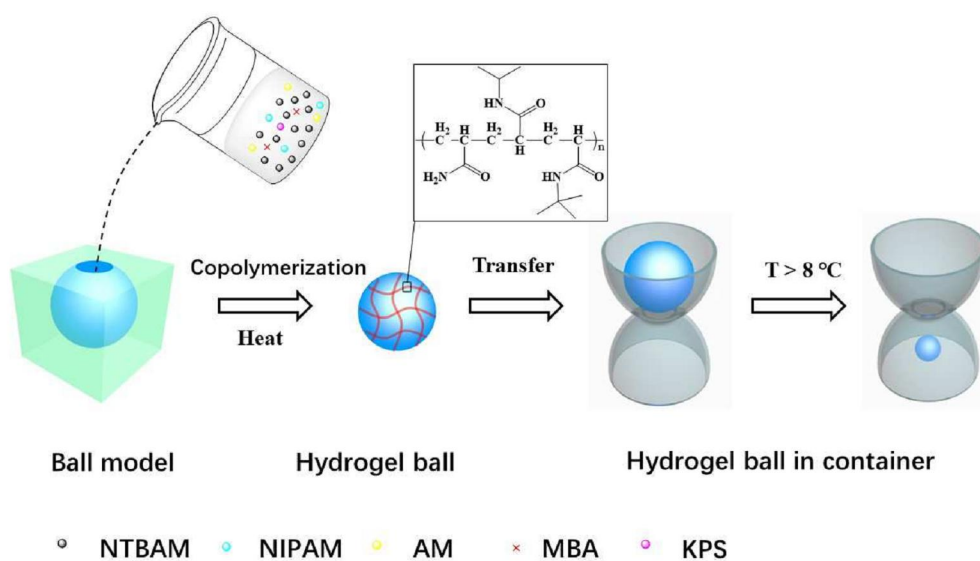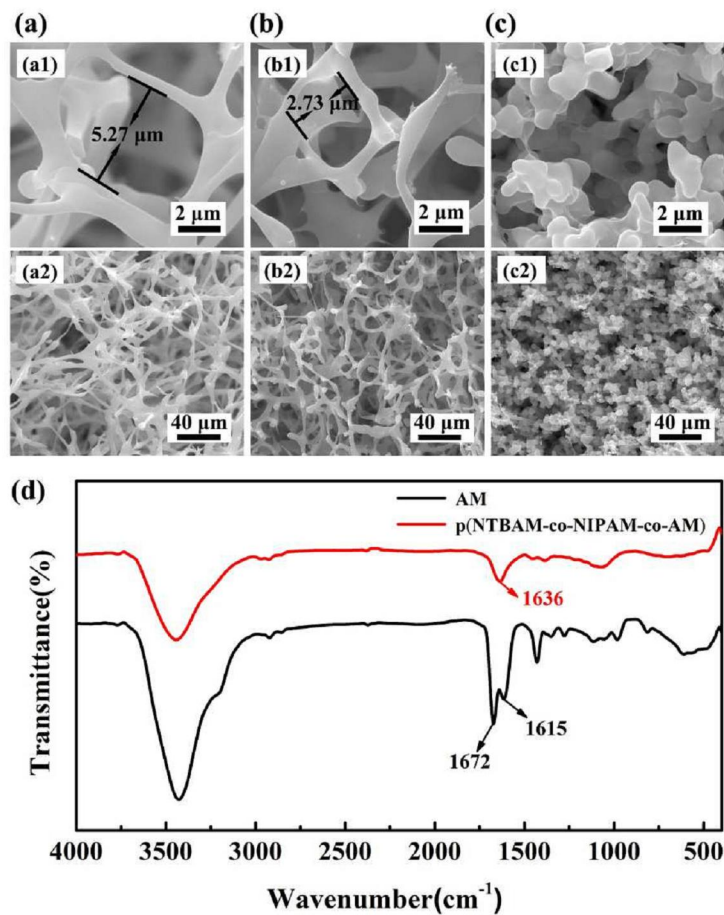
Figure 2. (a) Deswelling behaviors of p(NTBAM-co-NIPAM-co-AM) hydrogel. (b) Diameter change and distribution of p(NTBAM-co-NIPAM-co-AM) hydrogel at a range of temperature change windows from 2 to 26 ℃. (c) Swelling kinetics of pNTBAM, pNIPAM, and p(NTBAM-co-NIPAM-co-AM) hydrogels at 10 ℃.
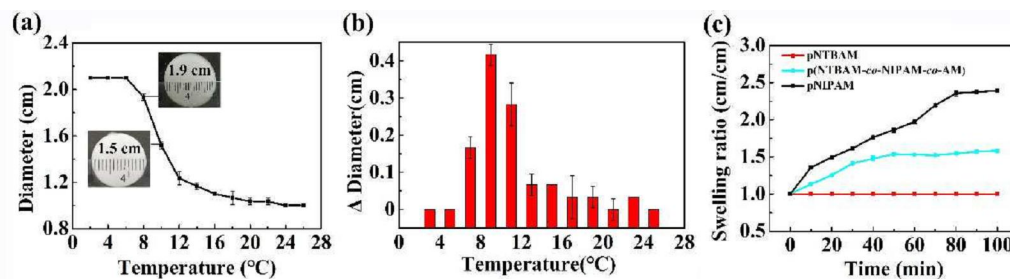
Figure 3. SEM cross-sectional images of p(NTBAM-co-NIPAM-co-AM) hydrogels by swelling at 2 ☐ and de-swelling at different temperatures of (a) 4 ☐, (b) 10 ☐, and (c) 26 ☐. (d) FT-IR spectra of AM monomer and p(NTBAM-co-NIPAM-co-AM) hydrogels.

Figure 4. (a) DSC thermograms of p(NTBAM-co-NIPAM-co-AM) hydrogels with different LCST, Gel a hydrogel with LCST of 6 □, Gel b hydrogel with LCST of 8 □, Gel c hydrogel with LCST of 12 ⌐, Gel d hydrogel with LCST of 18 □; (b) Glass transition temperature dependence on LCST of p(NTBAM-co-NIPAM-co-AM) hydrogels.
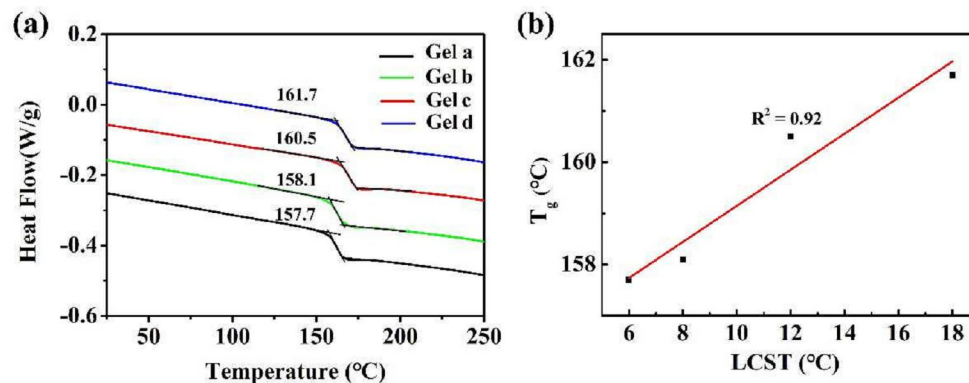
Figure 5. Concentration effect of MBA crosslinker on (a) deswelling behaviors and (b) diameter change and distribution of p(NTBAM-co-NIPAM-co-AM) hydrogels at a range of temperature change windows from 2 to 26 ☐. (c) Compressive stress-strain curves for p(NTBAM-co-NIPAM-co-AM) hydrogels with different MBA crosslinker concentrations. All hydrogels were prepared at NTBAM of 0.525 mmol/ml, NIPAM of 0.15mmol/ml, and AM of 0.25mmol/ml.
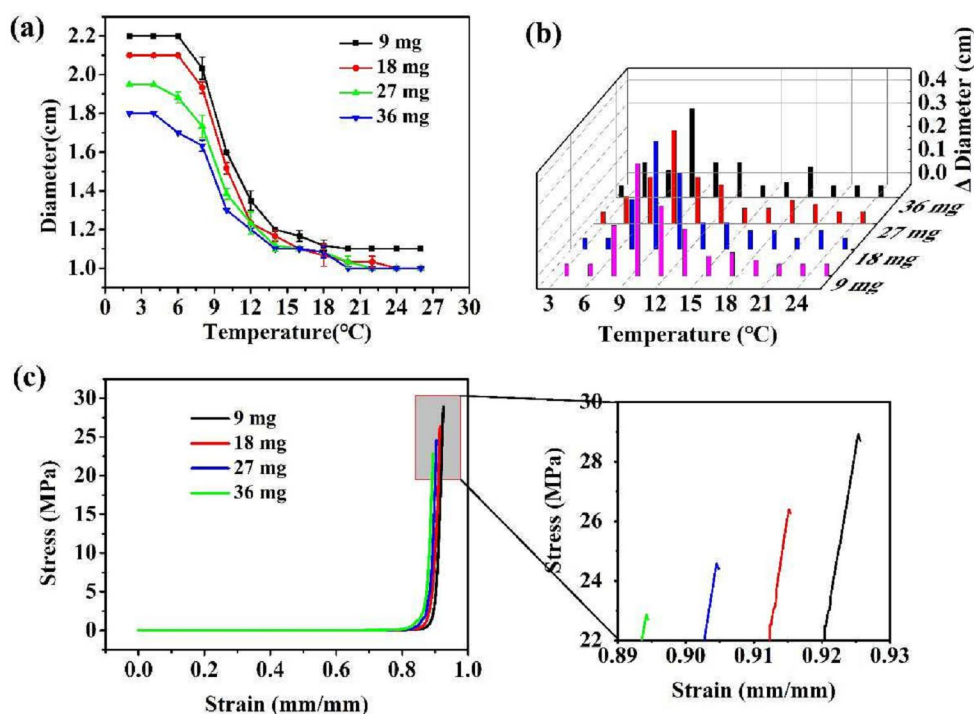
Figure 6. A p(NTBAM-co-NIPAM-co-AM) hydrogel ball experienced a size change from 1.9 cm to 1.5 cm at 8□ to10□, thus could be used as a temperature-responsive hydrogel actuator.
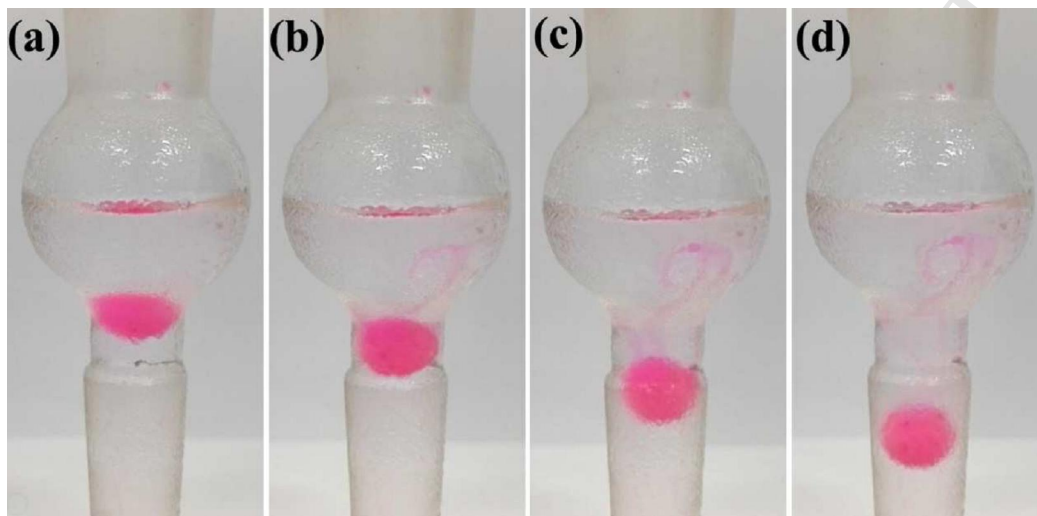
Table of Content
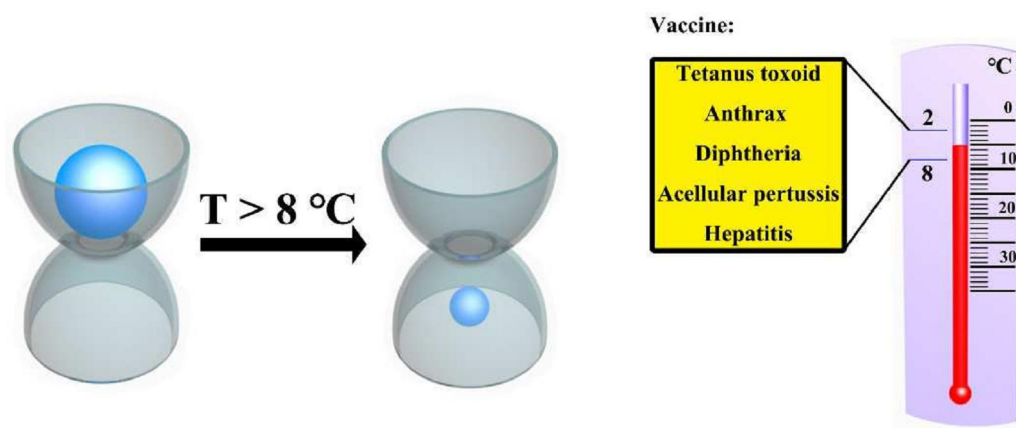
References

[1] S. Plotkin, History of vaccination, Proceedings of the National Academy of Sciences of the

United States of America 111(34) (2014) 12283-12287.

[2] M. Lombard, P.P. Pastoret, A.M. Moulin, A brief history of vaccines and vaccination, Revue

Scientifique et Technique de l'OIE 26(1) (2007) 29-48.

[3] W.H. Organization, Health: a key to prosperity: success stories in developing countries,

Health: a key to prosperity: success stories in developing countries, World Health Organization,

2000.

[4] M.J. Corbel, Reasons for instability of bacterial vaccines, Dev Biol Stand 87 (1996)

113-124.

[5] S.E. Zweig, Advances in vaccine stability monitoring technology, Vaccine 24(33) (2006)

5977-5985.

[6] W.F. Tonnis, J.P. Amorij, M.A. Vreeman, H.W. Frijlink, G.F. Kersten, W.L. Hinrichs,

Improved storage stability and immunogenicity of hepatitis B vaccine after spray-freeze drying

in presence of sugars, Eur J Pharm Sci 55 (2014) 36-45.

[7] O.S. Kumru, S.B. Joshi, D.E. Smith, C.R. Middaugh, T. Prusik, D.B. Volkin, Vaccine

instability in the cold chain: mechanisms, analysis and formulation strategies, Biologicals 42(5)

(2014) 237-59.

[8] L.D. Schlehuber, I.J. McFadyen, Y. Shu, J. Carignan, W.P. Duprex, W.R. Forsyth, J.H. Ho,

C.M. Kitsos, G.Y. Lee, D.A. Levinson, S.C. Lucier, C.B. Moore, N.T. Nguyen, J. Ramos, B.A.

Weinstock, J. Zhang, J.A. Monagle, C.R. Gardner, J.C. Alvarez, Towards ambient

temperature-stable vaccines: the identification of thermally stabilizing liquid formulations for

measles virus using an innovative high-throughput infectivity assay, Vaccine 29(31) (2011) 5031-5039.

[9] J. Lloyd, J. Cheyne, The origins of the vaccine cold chain and a glimpse of the future, Vaccine 35(17) (2017) 2115-2120.

[10] W.H. Organization, Getting started with vaccine vial monitors, Geneva: World Health Organization, 2002.

[11] W.H. Organization, How to monitor temperatures in the vaccine supply chain, World Health Organization, 2015.

[12] Y. Li, G. Huang, X. Zhang, B. Li, Y. Chen, T. Lu, T.J. Lu, F. Xu, Magnetic Hydrogels and Their Potential Biomedical Applications, Advanced Functional Materials 23(6) (2013) 660-672.

[13] C. Ma, W. Lu, X. Yang, J. He, X. Le, L. Wang, J. Zhang, M.J. Serpe, Y. Huang, T. Chen, Bioinspired Anisotropic Hydrogel Actuators with On-Off Switchable and Color-Tunable Fluorescence Behaviors, Advanced Functional Materials 28(7) (2017) 1704568.

[14] Z. Sun, Y. Yamauchi, F. Araoka, Y.S. Kim, J. Bergueiro, Y. Ishida, Y. Ebina, T. Sasaki, T. Hikima, T. Aida, An Anisotropic Hydrogel Actuator Enabling Earthworm-Like Directed Peristaltic Crawling, Angewandte Chemie International Edition 57(48) (2018) 15772-15776.

[15] L.-W. Xia, R. Xie, X.-J. Ju, W. Wang, Q. Chen, L.-Y. Chu, Nano-structured smart hydrogels with rapid response and high elasticity, Nature communications 4 (2013) 2226.

[16] Q. Xiao, Y. Li, F. Li, M. Zhang, Z. Zhang, H. Lin, Rational design of a thermalresponsive-polymer-switchable FRET system for enhancing the temperature sensitivity of upconversion nanophosphors, Nanoscale 6(17) (2014) 10179-86.

[17] H. Gu, H. Zhang, C. Ma, H. Sun, C. Liu, K. Dai, J. Zhang, R. Wei, T. Ding, Z. Guo, Smart

21

strain sensing organic–inorganic hybrid hydrogels with nano barium ferrite as the cross-linker, Journal of Materials Chemistry C 7(8) (2019) 2353-2360.

[18] S. Li, A. Jasim, W. Zhao, L. Fu, M.W. Ullah, Z. Shi, G. Yang, Fabrication of pH-electroactive Bacterial Cellulose/Polyaniline Hydrogel for the Development of a Controlled Drug Release System, ES Materials & Manufacturing 1 (2018) 41-49.

[19] X. Hu, R. Liang, J. Li, Z. Liu, G. Sun, Highly Stretchable Self-Healing Nanocomposite Hydrogel Reinforced by 5 nm Particles, ES Materials & Manufacturing 2 (2018) 16-23.

[20] E.S. Gil, S.M. Hudson, Stimuli-reponsive polymers and their bioconjugates, Progress in polymer science 29(12) (2004) 1173-1222.

[21] T. Still, P.J. Yunker, K. Hanson, Z.S. Davidson, M.A. Lohr, K.B. Aptowicz, A.G. Yodh, Temperature-Sensitive Hydrogel-Particle Films from Evaporating Drops, Advanced Materials Interfaces 2(16) (2015) 1500371.

[22] Y.-Y. Wei, Z. Liu, X.-J. Ju, K. Shi, R. Xie, W. Wang, Z. Cheng, L.-Y. Chu, Gamma-Cyclodextrin-Recognition-Responsive Characteristics of Poly(N-isopropylacrylamide)-Based Hydrogels with Benzo-12-crown-4 Units as Signal Receptors, Macromolecular Chemistry and Physics 218(1) (2017) 1600386.

[23] K. Kempe, T. Neuwirth, J. Czaplewska, M. Gottschaldt, R. Hoogenboom, U.S. Schubert, Poly(2-oxazoline) glycopolymers with tunable LCST behavior, Polymer Chemistry 2(8) (2011) 1737-1743.

[24] E.G. Gharakhanian, T.J. Deming, Role of Side-Chain Molecular Features in Tuning Lower Critical Solution Temperatures (LCSTs) of Oligoethylene Glycol Modified Polypeptides, J Phys Chem B 120(26) (2016) 6096-6101.

[25] Y.S. Chen, S.J. Yoon, W. Frey, M. Dockery, S. Emelianov, Dynamic contrast-enhanced photoacoustic imaging using photothermal stimuli-responsive composite nanomodulators, Nature communications 8 (2017) 15782.

[26] Y. Hiruta, M. Shimamura, M. Matsuura, Y. Maekawa, T. Funatsu, Y. Suzuki, E. Ayano, T. Okano, H. Kanazawa, Temperature-Responsive Fluorescence Polymer Probes with Accurate Thermally Controlled Cellular Uptakes, ACS Macro Letters 3(3) (2014) 281-285.

[27] Y. Hiruta, Y. Nagumo, Y. Suzuki, T. Funatsu, Y. Ishikawa, H. Kanazawa, The effects of anionic electrolytes and human serum albumin on the LCST of poly(N-isopropylacrylamide)-based temperature-responsive copolymers, Colloids Surf B Biointerfaces 132 (2015) 299-304.

[28] J. Lee, H. Yang, C.H. Park, H.-H. Cho, H. Yun, B.J. Kim, Colorimetric Thermometer from Graphene Oxide Platform Integrated with Red, Green, and Blue Emitting, Responsive Block Copolymers, Chemistry of Materials 28(10) (2016) 3446-3453.

[29] A. Choe, J. Yeom, R. Shanker, M.P. Kim, S. Kang, H. Ko, Stretchable and wearable colorimetric patches based on thermoresponsive plasmonic microgels embedded in a hydrogel film, NPG Asia Materials 10(9) (2018) 912-922.

[30] Y. Hiruta, R. Kanazashi, E. Ayano, T. Okano, H. Kanazawa, Temperature-responsive molecular recognition chromatography using phenylalanine and tryptophan derived polymer modified silica beads, The Analyst 141(3) (2016) 910-917.

[31] W. Wang, Y. Guan, Z. Li, F. He, Y. Huang, W. Song, J. Hu, "On-Off" Thermoresponsive Coating Agent Containing Salicylic Acid Applied to Maize Seeds for Chilling Tolerance, Plos One 10(3) (2015) e0120695.

[32] E. Ruel-Gariepy, J.C. Leroux, In situ-forming hydrogels—review of temperature-sensitive systems, Eur J Pharm Biopharm 58(2) (2004) 409-426.

[33] L. Klouda, Thermoresponsive hydrogels in biomedical applications: A seven-year update, Eur J Pharm Biopharm 97(Pt B) (2015) 338-349.

[34] M. Constantin, S. Bucatariu, V. Harabagiu, I. Popescu, P. Ascenzi, G. Fundueanu, Poly(N-isopropylacrylamide-co-methacrylic acid) pH/thermo-responsive porous hydrogels as self-regulated drug delivery system, Eur J Pharm Sci 62 (2014) 86-95.

[35] A. Prasannan, H.-C. Tsai, Y.-S. Chen, G.-H. Hsiue, A thermally triggered in situ hydrogel from poly(acrylic acid-co-N-isopropylacrylamide) for controlled release of anti-glaucoma drugs, Journal of Materials Chemistry B 2(14) (2014).

[36] D. Xu, H. Yu, Q. Xu, G. Xu, K. Wang, Thermoresponsive Photonic Crystal: Synergistic Effect of Poly(N-isopropylacrylamide)-co-acrylic Acid and Morpho Butterfly Wing, ACS applied materials & interfaces 7(16) (2015) 8750-8756.

[37] J. Herzberger, K. Niederer, H. Pohlit, J. Seiwert, M. Worm, F.R. Wurm, H. Frey, Polymerization of Ethylene Oxide, Propylene Oxide, and Other Alkylene Oxides: Synthesis, Novel Polymer Architectures, and Bioconjugation, Chemical reviews 116(4) (2016) 2170-2243.

[38] Y. Qu, X. Wei, Z. Qian, Thermosensitive Biomaterials in Tissue Engineering, Smart Materials for Tissue Engineering2016, pp. 418-440.

[39] N.K. Singh, D.S. Lee, In situ gelling pH- and temperature-sensitive biodegradable block copolymer hydrogels for drug delivery, J Control Release 193 (2014) 214-227.

[40] P. Wang, W. Chu, X. Zhuo, Y. Zhang, J. Gou, T. Ren, H. He, T. Yin, X. Tang, Modified PLGA–PEG–PLGA thermosensitive hydrogels with suitable thermosensitivity and properties

for use in a drug delivery system, Journal of Materials Chemistry B 5(8) (2017) 1551-1565.

[41] W.J. Lokerse, E.C. Kneepkens, T.L. ten Hagen, A.M. Eggermont, H. Grull, G.A. Koning, In depth study on thermosensitive liposomes: Optimizing formulations for tumor specific therapy and in vitro to in vivo relations, Biomaterials 82 (2016) 138-150.

[42] W.J.M. Lokerse, A.M.M. Eggermont, H. Grull, G.A. Koning, Development and evaluation of an isolated limb infusion model for investigation of drug delivery kinetics to solid tumors by thermosensitive liposomes and hyperthermia, J Control Release 270 (2018) 282-289.

[43] M.B. Huglin, M.M.A.M. Rehab, Mechanical and thermodynamic properties of butyl acrylate-N-vinylpyrrolidone hydrogels, Polymer 28(13) (1987) 2200-2206.

[44] B. Yildiz, B. Işik, M. Kiş, Thermoresponsive poly(N-isopropylacrylamide-co-acrylamide-co-2-hydroxyethyl methacrylate) hydrogels, Reactive and Functional Polymers 52(1) (2002) 3-10.

[45] W. Funke, O. Okay, B. Joosmüller, Microgels-Intramolecularly Crossünked Macromolecules with a Globular Structure, Advances in Polymer Science 136 (1998) 139-234.

Demonstration of high temperature sensitivity (~2 ℃), large volume deswelling ratio (90%), and low temperature-responsive range (8-10 ℃) for temperature-responsive hydrogels acting as temperature indicator for vaccine-related applications.